Single Crystal 55 Mn ENDOR of Concanavalin A: Detection of Two Mn 2+ Sites with Different 55 Mn Quadrupole Tensors

3 **AUTHORS**, INCLUDING:

Kv Narasimhulu
Tampa, USA

46 PUBLICATIONS   **885** CITATIONS

Raanan Carmielli
Weizmann Institute of Science

44 PUBLICATIONS   **866** CITATIONS

Single Crystal ^{55}Mn ENDOR of Concanavalin A: Detection of Two Mn^{2+} Sites with Different ^{55}Mn Quadrupole Tensors

Kuppala V. Narasimhulu, Raanan Carmieli, and Daniella Goldfarb*

Contribution from the Departments of Chemical Physics, The Weizmann Institute of Science, Rehovot Israel 76100

Received August 30, 2006; E-mail: daniella.goldfarb@weizmann.ac.il

Abstract: Concanavalin A is a member of the plant hemeagglutinin (or plant lectin) family that contains two metal binding sites; one, called S1, is occupied by Mn^{2+} and the other, S2, by Ca^{2+}. ^{55}Mn electron–nuclear double resonance (ENDOR) measurements were performed on a single crystal of concanavalin A at W-band (95 GHz, ~3.5 T) to determine the ^{55}Mn nuclear quadrupole interaction in a protein binding site and its relation to structural parameters. Such measurements are easier at a high field because of the high sensitivity for size-limited samples and the reduction of second-order effects on the spectrum which simplifies spectral analysis. The analysis of the ^{55}Mn ENDOR rotation patterns showed that two chemically inequivalent Mn^{2+} types are present at low temperatures, although the high-resolution X-ray structure reported only one site. Their quadrupole coupling constants, e^2Qq/h, are significantly different; 10.7 ± 0.6 MHz for Mn$_A^{2+}$ and only −2.7 ± 0.6 MHz for Mn$_B^{2+}$. The ENDOR data also refined the hyperfine coupling determined earlier by single-crystal EPR measurements, yielding a small but significant difference between the two: −262.5 MHz for Mn$_A^{2+}$ and −263.5 MHz for Mn$_B^{2+}$. The principal z-axis for Mn$_A^{2+}$ is not aligned with any of the Mn-ligand directions, but is 25° off the Mn-asp10 direction, and its orientation is different than that of the zero-field splitting (ZFS) interaction. Because of the small quadrupole interaction of Mn$_B^{2+}$ the orientation dependence was very mild, leading to larger uncertainties in the asymmetry parameter. Nonetheless, there too z is not along the Mn-ligand bonds and is rotated 90° with respect to Mn$_A$. These results show, that similar to the ZFS, the quadrupolar interaction is highly sensitive to small differences in the coordination sphere of the Mn^{2+}, and the resolution of the two types is in agreement with the earlier observation of a two-site conformational dynamic detected through the ZFS interaction, which is frozen out at low temperatures and averaged at room temperature. To account for the structural origin of the different e^2Qq/h values, the electric field gradient tensor was calculated using the point-charge model. The calculations showed that a relatively small displacement of the oxygen ligand of asp10 can lead to differences on the order observed experimentally.

Introduction

Single-crystal high-field EPR and electron–nuclear double resonance (ENDOR) spectroscopy have been shown to be most useful in the studies of paramagnetic metal binding sites in proteins, particularly owing to the high sensitivity for size-limited samples.[1–7] Single crystal measurements provide the complete magnetic tensors, namely principal components and orientation, and thereby supply spatial and electronic structural information on the metal site. Recently, we have investigated

the Mn^{2+} site in single crystals of the protein concanavalin A to demonstrate the feasibility of the method. Concanavalin A is a member of the plant hemeagglutinin (or plant lectin) family; a large and ubiquitous group of saccharide-binding proteins.[8] The importance of these proteins is expressed in their ability to bind saccharides; each member of the family has a unique saccharide specificity.[8] The three-dimensional (3D) structure of concanavalin A has been determined at an exceptionally high resolution, 0.94 Å, at low temperature.[9] The crystal has an orthorhombic symmetry (space group I_{222}), with unit cell parameters $a = 89.2$, $b = 87.2$, and $c = 62.9$ Å. It forms a tetramer of 100 kDa total molecular weight. Each monomer has two metal binding sites; one, called S1, is occupied by Mn^{2+}, and the other, S2, by Ca^{2+}, as shown in Figure 1. The occupancy of both sites is essential for saccharide binding.[10] The Mn^{2+} site has a slightly distorted octahedral geometry in which the

(1) Coremans, J. W. A.; Poluektov, O. G.; Groenen, E. J. J.; Canters, G. W.; Nar, H.; Messerschmidt, A. *J. Am. Chem. Soc.* **1994**, *116*, 3097–3101.
(2) Groenen, E. J. J.; Canters, G. W.; Nar, H.; Coremans, J. W. A.; Poluektov, O. G.; Messerschmidt, A. *J. Am. Chem. Soc.* **1996**, *118*, 12141–12153.
(3) Manikandan, P.; Carmieli, R.; Shane, T.; Kalb (Gilboa), A. J.; Goldfarb, D. *J. Am. Chem. Soc.* **2000**, *122*, 3488–3494.
(4) Carmieli, R.; Manikandan, P.; Kalb, A. J.; Goldfarb, D. *J. Am. Chem. Soc.* **2001**, *123*, 8378–8386.
(5) Carmieli, R.; Manikandan, P.; Epel, B.; Kalb, A. J.; Schnegg, A.; Savitsky, A.; Mobius, K.; Goldfarb, D. *Biochemistry* **2003**, *42*, 7863–7870.
(6) Hogböm, M.; Galander, M.; Andersson, M.; Kolberg, M.; Hofbauer, W.; Lassmann, G.; Nordlund, P.; Lendzian, F. *Proc. Nat. Acad. Sci. U.S.A.* **2003**, *100*, 3209–3214.
(7) Fittipaldi, M.; Steiner, R. A.; Matsushita, M.; Dijkstra, B. W.; Groenen, E. J. J.; Huber, M. *Biophysical. J.* **2003**, 4047–4054.

(8) Kalb (Gilboa), A. J.; Habash, J; Hunter, N. S.; Price, H. J.; Raftery, J, Helliwell, J. R. *Metal Ions in Biological Systems*; Sigel, A., Sigel, H., Eds.: Marcel Dekker Inc.: New York, 2000; Vol. 37.
(9) Deacon, A.; Gleichmann, T.; Kalb (Gilboa), A. J. *J. Chem. Soc., Dalton Trans.* **1997**, *93*, 4305–4312.
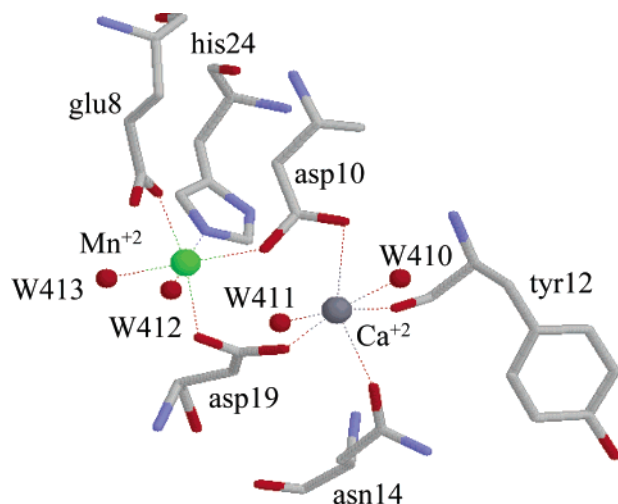
Figure 1. The structure of the Mn^{2+} and Ca^{2+} sites in concanavalin A as determined from X-ray crystallographic data.[9]

Mn^{2+} is coordinated to the carboxyl groups of asp10, asp19, glu8, the imidazole N_ϵ of his24, and two water molecules. The role of the transition metal in this protein is structural, and the Mn^{2+}, together with the Ca^{2+} serve as stabilizers for the loops that constitute the saccharide binding site.

The zero-field splitting (ZFS) of the Mn^{+2} ion was first determined at room temperature by single-crystal Q-band continuous wave (CW) EPR spectroscopy.[11] Further W-band (95 GHz, ~3.5 T) EPR investigations showed that at room temperature the crystals contain one type of Mn^{2+}, consistent with the reported 3D structure, but at low temperatures two Mn^{2+} types were resolved and their ZFS tensors were determined.[5] Temperature dependence experiments showed that a two-site exchange process takes place. At room-temperature this interconversion is fast on the EPR time scale and one averaged site is observed. This dynamic process was attributed to a conformational equilibrium at the Mn^{2+} site, most probably due to a local motion of one (or more) of its ligands. Low-temperature W-band single crystal ^1H ENDOR measurements[4] provided the location of two protons of the imidazole ring and of the water ligands and the involvement of the latter in hydrogen bonds with nearby residues. The observation of only one type of protons for each water ligand and for the imidazole protons indicates that neither the water nor the histidine ligand are involved in the conformational equilibria.

In the present study, we have investigated the ^{55}Mn ENDOR of single crystals of concanavalin A to further refine the ^{55}Mn hyperfine coupling obtained from the EPR measurements, which was found to be the same for both Mn^{2+} types,[5] and, more importantly to determine their ^{55}Mn quadrupole tensors. The question that arises is whether the ^{55}Mn quadrupole interaction can also resolve the two states sensed by the ZFS and whether it can provide additional insight into the specific dynamic involved. Moreover, to the best of our knowledge the full ^{55}Mn nuclear quadrupole has not been determined in a protein binding site, and therefore the concanavalin A results can serve as a reference for future studies on Mn^{2+} binding sites.

The analysis of $^{55}Mn^{2+}$ ENDOR spectra at X-band frequencies has been described in detail by Britt and co-workers.[12] In this analysis the isotropic hyperfine interaction and the nuclear Zeeman interactions were considered, while the ZFS has been neglected, although it has been suggested that it can lead to line broadening. When the ZFS is substantial compared to the Zeeman interaction, it introduces additional anisotropy into the ENDOR spectra of high spin d^5 ions.[13-15] This is, however, significantly reduced at high fields.[16] A recent report on pulsed ENDOR at 275 GHz on a single crystal of 0.2% Mn^{2+} in $ZnGeP_2$ has clearly revealed the quadrupolar splitting.[17] In contrast, W-band ^{55}Mn ENDOR spectra of a number of Mn substituted aluminophosphate molecular sieves could resolve different Mn^{2+} types on the basis of their different hyperfine couplings, but the quadrupole splittings could not be resolved because the samples investigated were polycrystalline and the ENDOR lines were too broad.[18] X-band pulsed ENDOR measurement on a series of vanadyl complexes in frozen solutions provided the quadrupole coupling constant of ^{51}V and showed that it is sensitive to the ligand environment of the complexes.[19-21] This is a $S = \frac{1}{2}$ system and therefore, the ZFS effects are of no concern and the need for high field is not so crucial. Nonetheless, also for $S = \frac{1}{2}$, the second-order effects of the hyperfine and quadrupole interactions are substantially reduced at high field.

In this manuscript, we first present a brief theoretical background and give the expressions for the ENDOR frequencies, addressing the contribution of the ZFS on the basis of third-order perturbation theory, followed by the presentation of the ^{55}Mn ENDOR results and their analysis. Similar to the EPR measurements, which revealed the presence of two different ZFS tensors, the ENDOR spectra disclosed two Mn^{2+} types with different nuclear quadrupole interactions, showing that the electric field gradient (efg) at the Mn^{2+} site is also highly sensitive to subtle changes in ligands conformation. Further calculations of the efg, based on the point-charge model showed that the differences between the two sites can be accounted for by a change in the position and charge of the coordinated oxygen of the bridging carboxylate of asp10.

Experimental

Crystal Growth and Mounting. Crystals were grown and inserted into the W-band tubes as described earlier.[3,4] The single crystals were mounted into thin-walled quartz capillary tubes (outer diameter 0.7 mm) with two orientations, one with the *b*-axis parallel to the tube axis, for acquiring EPR and ENDOR rotation patterns in the *ac* plane, and the other with the *c*-axis parallel to the tube axis for *ab* plane measurements.

(10) Becker, J. W.; Reeke, G. N., Jr.; Wang, J. L.; Cunningham, B. A.; Edelman, G. M. *J. Biol. Chem.* **1975**, *250*, 1513−1524.
(11) Meirovitch, E.; Luz, Z.; Kalb, A. J. *J. Am. Chem. Soc.* **1974**, *96*, 7538−7541.
(12) Sturgeon, B. E.; Bell, J. A.; Randall, D. W.; Britt, R. D. *J. Phys. Chem.* **1994**, *98*, 12871−1283.
(13) Vardi, R.; Bernardo, M.; Thomman, H.; Strohmaier, K. G.; Vaughan, D. E. W.; Goldfrab, D. *J. Magn. Reson.* **1997**, *126*, 229−241.
(14) Astashkin, A. V.; Raitsimring, A. M. *J. Chem. Phys.* **2002**, *117*, 6121−6132.
(15) Astashkin, A. V.; Raitsimring, A. M.; Caravan, P. *J. Phys. Chem. A* **2004**, *108*, 1990−2001.
(16) Goldfarb, D.; Strohmaier, K. G.; Vaughan, D. E. W.; Thomann H.; Poluektov O. G.; Schmidt J. *J. Am. Chem. Soc.* **1996**, *118*, 4665−4671.
(17) Blok, H.; Disselhorst, J. A. J. M.; van der Meer, H.; Orlinskii, S. B.; Schmidt, J. *J. Magn. Reson.* **2005**, *173*, 49−53.
(18) Arieli, D.; Prisner, T. F.; Hertel, M.; Goldfarb, D. *Phys. Chem. Chem. Phys.* **2004**, *6*, 172−181.
(19) Anzar, C. P.; Deligiannakis, Y.; Tolis, E. J.; Kabanos, T.; Brynda, M.; Britt, R. D. *J. Phys. Chem. A* **2004**, *108*, 4310−4321.
(20) Grant, C. V.; Ball, J. A.; Hamstra, B. J.; Pecoraro, V. L.; Britt, R. D. *J. Phys. Chem. B* **1998**, *102*, 8145−8150.
(21) Grant, C. V.; Geiser-Bush, K. M.; Corman, C. R.; Britt, R. D. *Inorg. Chem.* **1999**, *38*, 6285−6288.
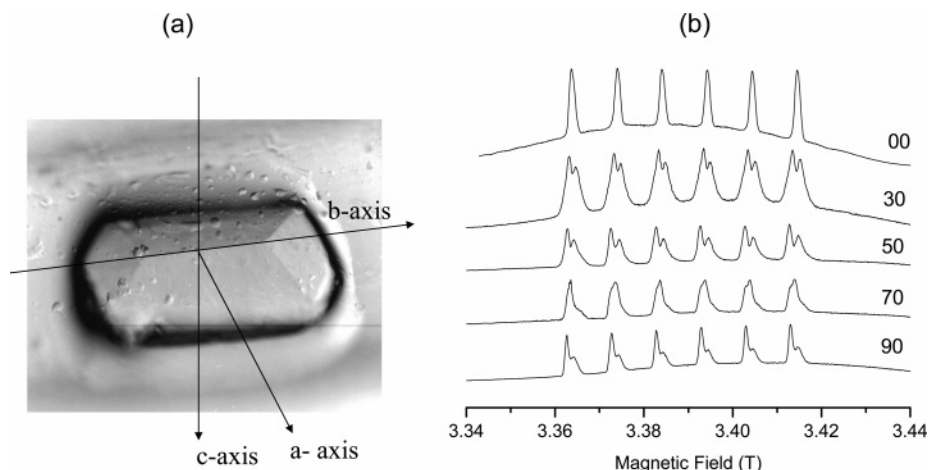
Figure 2. (a) The morphology of the concanavalin A crystal and the crystallographic axes directions. The *b*-axis is along the longest growth direction; *c*-axis is in the plane perpendicular to the *b*-axis on the surface of the crystal. (b) Example FS-ED EPR spectra of concanavalin A in *ac* plane measured at 6 K. The notation angles are noted on the figure.

The crystals had a regular morphology, and the relation between the morphology and the crystallographic axis, as determined by X-ray diffraction measurements on a single-crystal diffractometer, is shown in Figure 2. The regular morphology considerably facilitated mounting the crystals with the desired orientation in the tube. Typical crystal sizes were $(0.4-0.7) \times 0.4 \times 0.3$ mm³

Pulsed-EPR and ENDOR Measurements. W-band pulsed experiments (94.9 GHz) were carried out on a home-built spectrometer at 6 K.[22] The field-swept echo-detected (FS-ED) EPR spectra were obtained using the two-pulse echo sequence $(\pi/2-\tau-\pi-\tau-\text{echo})$ with pulses of 30 and 60 ns, $\tau = 250$ ns, and a repetition time of 3 ms. The ENDOR rotation patterns were collected on the lowest field ⁵⁵Mn hyperfine component corresponding to the $|-\frac{1}{2}, -\frac{5}{2}\rangle \rightarrow |+\frac{1}{2}, -\frac{5}{2}\rangle$ EPR transition. The Davies ENDOR sequence $(\pi-T-\pi/2-\tau-\pi-\tau-\text{echo})$, with a RF pulse applied during the time T, was used with π and $\pi/2$ MW (microwave) pulse lengths of 60 and 30 ns, respectively. The RF pulse length t_{RF} was 15 μs, the repetition time equal to 5 ms, and τ equal to 300 *ns*. The magnetic field was calibrated using the ¹H Larmor frequency obtained from Mims or Davies ¹H ENDOR spectra. Whenever the individual hyperfine components of the different Mn²⁺ sites were resolved in the EPR spectrum, ENDOR spectra were recorded setting the field to each of the resolved features.

Simulations. The ⁵⁵Mn ENDOR rotation patterns of the $M_S = \pm\frac{1}{2}$ manifolds were simulated using an in house Matlab program based on the equations presented in the next section.

DFT Calculations. Single point DFT (density functional theory) calculations were performed with ORCA using four functionals (B3LYP, B86, B1P, B3PW91).[23] The basis sets employed were the accurate triply polarized basis set CP(PPP) with an appropriate integration grid for Mn,[24] triple-ζ quality basis set (TZV) from Ahlrichs[25] for the Ca and the atoms of the first coordination sphere of both metals, and the SV basis set for all other atoms. The charges were obtained from natural population analysis using an algorithm implemented in the NBO 5.0 program.[26] The four different functionals produced similar charge distribution.

Theory

Initially we obtained expressions for ENDOR frequencies derived from third-order perturbation theory, using a Hamiltonian which does not include the quadrupole interaction but

(22) Gromov, I.; Krymov, V.; Manikandan, P.; Arieli, D.; Goldfarb, D. *J. Magn. Reson.* **1999**, *139*, 8−17.
(23) Neese F. *ORCA − an ab Initio, Density Functional and Semiempirical Program Package*, version 2.5; University of Bonn: Bonn, Germany, 2006.
(24) Neese, F. *Inorg. Chim. Acta* **2002**, *337C*, 181−192.
(25) Schaefer, A.; Horn, H.; Ahlrichs, R. *J. Chem. Phys.* **1992**, *97*, 2571−2577.

includes the ZFS to evaluate its contribution to the ENDOR frequencies. Earlier X-band ENDOR measurements on ⁵⁷Fe-(III) in zeolites showed that when the hyperfine coupling and the ZFS are significant with respect to the electron Zeeman interaction, the ENDOR frequencies contain a contribution from the ZFS.[14,13] The effect of the ZFS on the nuclear modulation frequencies at X-band frequencies for high spin Gd(III) has been noted as well.[14] The third-order expressions for the ENDOR frequencies, including the nuclear Zeeman interaction in the high-order terms, neglected previously,[13] are given in the Supporting Information. Taking $a_{iso} = -265$ MHz, $D = 970$ MHz, and $E/D = 0.15$, which are the values obtained for Mn$_A$ in concanavalin A at low temperatures,[5] we calculated the orientation dependence of the third-order contributions to the sums and differences of the ENDOR frequencies of the $M_S = \pm\frac{1}{2}$ levels, given by $\nu_+(\frac{1}{2})$ and $\Delta\nu(\frac{1}{2})$, respectively (see Supporting Information). It shows that the shifts expected are of the order of 0.1 MHz, which is within the line width, and therefore the effect of the ZFS can be neglected. Third-order corrections due to the hyperfine interaction are also small and negligible.

The ⁵⁵Mn ENDOR spectra of concanavalin A, however, do exhibit a significant orientation dependence (see below) which must arise from the nuclear quadrupole interaction. The spin-Hamiltonian considered for calculating the ENDOR frequencies was the following:

$$\mathcal{H} = \nu_o S_z - \nu_I I_z + a_{iso} S_z I_z + \frac{1}{2} a_{iso}[S_+ I_- + S_- I_+] +$$
$$F\left[I_z^2 - \frac{1}{3} I(I+1)\right] + G_+ [I_+ I_z + I_z I_+] +$$
$$G_- [I_- I_z + I_z I_-] + K_+ I_+^2 + K_- I_-^2 \quad (1)$$

where ν_0 and ν_I are the electron and nucleus Larmor frequencies, respectively, and

$$F = P\left[\frac{1}{2}(3\cos^2\theta - 1) + \frac{1}{2}\eta \sin^2\theta \cos 2\phi\right]$$

(26) Glendening, E. D.; Badenhoop, J. K.; Reed, A. E.; Carpenter, J. E.; Bohmann, J. A.; Morales, C. M.; Weinhold F. *NBO 5.0*; Theoretical Chemistry Institute, University of Wisconsin: Madison, WI, 2001; http://www.chem.wisc.edu/~nbo5.

$$G_\pm = P/4\left[-\sin 2\theta + \frac{1}{3}\eta \sin 2\theta \cos 2\phi \pm i\frac{2}{3}\eta \sin \theta \sin 2\phi\right]$$

$$K_\pm =$$
$$P/4\left[\sin^2 \theta + \frac{1}{3}\eta(\cos^2 \theta + 1) \cos 2\phi \pm i\frac{2}{3}\eta \cos \theta \sin 2\phi\right] \quad (2)$$

In eq 2, $P = {}^3/_2 P_{zz}$, $P_{zz} = (e^2 Qq/h2I(2I - 1))$, $\eta = (P_{xx} - P_{yy})/P_{zz}$, and P_{zz}, P_{yy}, and P_{xx}, are the principal components of the quadrupole tensor, **P**. The angles θ and ϕ define polar and azimuthal angles of the magnetic field with respect to the principal axis system of **P**. To first order, the ENDOR frequencies of the $M_S = \pm^1/_2$ manifolds are

$$\nu\left(\pm\frac{1}{2}\right)^{(1)} = \mp\frac{1}{2}a_{\text{iso}} + \nu_I - F(2M_I - 1) \quad (3)$$

The observed frequencies are always positive and therefore for the case of strong coupling, $|^1/_2 a_{\text{iso}}| > |\nu_I|$, as found in ^{55}Mn at W-band, the sum ENDOR frequency, ν_+, and the frequency splitting between the ENDOR transitions, $\Delta\nu$, for a given M_S value are

$$\nu_+ (|M_S|)^{(1)} = 2M_S a_{\text{iso}}, \quad \Delta\nu(|M_S|)^{(1)} = 2\nu_I \quad (4)$$

The second order correction terms for the ENDOR frequencies for each M_I value are

$$\nu\left(\pm\frac{1}{2},\frac{5}{2}\right)^{(2)} = \frac{a_{\text{iso}}^2}{4\nu_0}(17 \pm 4) + \frac{128G_+G_-}{\nu_I} - \frac{16K_+K_-}{\nu_I}$$

$$\nu\left(\pm\frac{1}{2},\frac{3}{2}\right)^{(2)} = \frac{a_{\text{iso}}^2}{4\nu_0}(17 \pm 2) - \frac{16G_+G_-}{\nu_I} + \frac{20K_+K_-}{\nu_I}$$

$$\nu\left(\pm\frac{1}{2},\frac{1}{2}\right)^{(2)} = \frac{17a_{\text{iso}}^2}{4\nu_0} - \frac{64G_+G_-}{\nu_I} + \frac{32K_+K_-}{\nu_I}$$

$$\nu\left(\pm\frac{1}{2},-\frac{3}{2}\right)^{(2)} = \frac{a_{\text{iso}}^2}{4\nu_0}(17 \mp 2) - \frac{16G_+G_-}{\nu_I} + \frac{20K_+K_-}{\nu_I}$$

$$\nu\left(\pm\frac{1}{2},-\frac{5}{2}\right)^{(2)} = \frac{a_{\text{iso}}^2}{4\nu_0}(17 \mp 4) + \frac{128G_+G_-}{\nu_I} - \frac{16K_+K_-}{\nu_I} \quad (5)$$

In the above equations, terms proportional to P^2/ν_0 were neglected because they are extremely small. Neglecting the second-order contribution of the quadrupole interaction, the expression for $\nu(\pm^1/_2)$ becomes

$$\nu\left(\pm\frac{1}{2}\right) = \mp\frac{1}{2}a_{\text{iso}} + \nu_I + \frac{17a_{\text{iso}}^2}{4\nu_0} + \left(-F \pm \frac{a_{\text{iso}}^2}{4\nu_0}\right)(2M_I - 1) \quad (6)$$

According to eq 6, any deviation of $\Delta\nu$ from $2\nu_I$ indicates that higher order hyperfine terms are important and/or that the nuclear quadrupole interaction is significant.

The expressions for $\Delta\nu(^1/_2, M_I)$ up to second-order corrections in both hyperfine and quadrupole interactions are

$$\Delta\nu\left(\frac{1}{2},\frac{5}{2}\right) = \Delta\nu\left(\frac{1}{2},-\frac{3}{2}\right) = 2\nu_I \mp 8F + \frac{17a_{\text{iso}}^2}{2\nu_0} + \frac{256B_+B_-}{\nu_I} - \frac{32C_+C_-}{\nu_I}$$

$$\Delta\nu\left(\frac{1}{2},\frac{3}{2}\right) = \Delta\nu\left(\frac{1}{2},-\frac{1}{2}\right) = 2\nu_I \mp 4F + \frac{17a_{\text{iso}}^2}{2\nu_0} - \frac{32B_+B_-}{\nu_I} + \frac{40C_+C_-}{\nu_I}$$

$$\Delta\nu\left(\frac{1}{2},\frac{1}{2}\right) = 2\nu_I + \frac{17a_{\text{iso}}^2}{2\nu_0} - \frac{128B_+B_-}{\nu_I} + \frac{64C_+C_-}{\nu_I} \quad (7)$$

Further measurements of the differences

$$\Delta\nu\left(\frac{1}{2},\frac{5}{2}\right) - \Delta\nu\left(\frac{1}{2},-\frac{3}{2}\right) = 16F$$

$$\Delta\nu\left(\frac{1}{2},\frac{3}{2}\right) - \Delta\nu\left(\frac{1}{2},-\frac{1}{2}\right) = 8F \quad (8)$$

yield a convenient, first-order dependence on the quadrupolar coupling, which was used to determine the ^{51}V $(I = {}^7/_2)$ quadrupolar splitting in a number of vanadyl complexes.[20] $\nu_+(^1/_2, M_I)$ has no contribution from the quadrupole interaction and therefore $\nu_+(^1/_2, {}^1/_2)$ should be used to determine a_{iso}.

In the single crystal measurements, we used the following reference frames:[5] the principal axis system of the magnetic tensor, $M(x, y, z)$, the crystal frame $C(c, a, b)$, the sample tube frame $T(x', y', z')$, where z' is parallel to the tube axis, the goniometer frame $G(x, y, z)$, and the lab frame $B(X, Y, Z)$, where $Z \| \vec{B}$. The transformation between these axis systems is done using the appropriate Euler angles and the corresponding Wigner rotation matrices, $R(\alpha', \beta', \gamma')$. For our experimental setup the transformations are

$$M \xrightarrow{\alpha,\beta,\gamma} C \xrightarrow{\phi',\theta',\psi} T \xrightarrow{0,0,\phi_0} G \xrightarrow{\phi_r,90,0} B \quad (9)$$

The rotation patterns are acquired by measuring the spectrum as a function of the rotation angle of the goniometer, ϕ_r. The relation between the above sets of angles and the angles θ and ϕ used in eq 2 is

$$R(-\phi, -\theta, 0) =$$
$$R(\phi_r, 90, 0) \, R(0, 0, \phi_0) \, R(\phi', \theta', \psi) \, R(\alpha, \beta, \gamma) \quad (10)$$

All angles in eq 10, except for α, β and γ, are defined by the experimental conditions.

There are four Mn^{2+} centers per unit cell in the crystals of concanavalin A[9] and, according to the I_{222} space group, their α, β, and γ are related as described in Table 1. To display the orientation of the ZFS, determined relative to the $C(c, a, b)$ axis system, in the atomic coordinate system (c, b, a) an additional transformation of $R(-90, -90, 90)$ was carried out. We chose to adhere to the $C(c, a, b)$ axis system for consistency

Table 1. The Euler Angles Relating the Principal Axis System of the Magnetic Tensors with the Crystallographic Axis System for the Four Different Mn^{2+} Sites of Concanavalin A

	α	β	γ
site I	α	β	γ
site II	α	β	$\gamma + 180$
site III	$180 + \alpha$	$180 - \beta$	$180 - \gamma$
site IV	$180 + \alpha$	$180 - \beta$	$-\gamma$

with the earlier single-crystal Q-band and W-band studies reported previously.[11,5]

Results

Single crystals of concanavalin A with a well-defined morphology (see Figure 2a) were oriented with the *b*-axis or *c*-axis parallel to the sample tube axis (perpendicular to the direction of the external magnetic field), and first ^{55}Mn EPR spectra were recorded as a function of the tube orientation in the *ac* and *ab* planes, respectively. According to the I_{222} space group, for each type of Mn^{2+} there are four symmetry-related sites and therefore at an arbitrary field orientation signals from four Mn^{2+} are expected. When the magnetic field is in any of the crystallographic planes, only two of the four sites are resolved since two pairs exhibit the same signals. When the field is along a crystallographic axis then all four become identical and only one signal is observed. The spectra obtained were the same as those reported earlier[5] and a few typical FS-ED EPR spectra in the *ac* plane are shown in Figure 2b. The EPR spectra show the six ^{55}Mn hyperfine components of the central $|-1/2, M_I\rangle \leftrightarrow |1/2, M_I\rangle$ EPR transition, often with a fine structure resolving different Mn^{2+} sites, superimposed on a broad background attributed to the other EPR transitions. The latter are not resolved because of distribution in ZFS, often referred to as strain. The EPR spectra showed more signals than expected from the I_{222} symmetry described above, thus revealing two types on Mn^{2+}.[5]

Recording the ^{55}Mn ENDOR spectrum with the field set to any of the central M_I transitions, should, in principle have contributions from the other EPR transitions as well. These, however, appear at much higher frequencies[12] and are outside the range of our RF amplifier. The ENDOR spectra were collected with the magnetic field set to the lowest field ^{55}Mn hyperfine component, $M_I = -5/2$. At this field, the ENDOR spectrum consists of only two lines, corresponding to the nuclear $|-5/2\rangle \leftrightarrow |-3/2\rangle$ transition within the $M_S = \pm 1/2$ manifolds, as illustrated for the EPR transition labeled a in Figure 3. Similarly, selecting the highest field ^{55}Mn hyperfine component results in the appearance of the $M_I |5/2\rangle \leftrightarrow |3/2\rangle$ ENDOR transitions of these M_S manifolds. In contrast, selecting any of the other hyperfine components leads to the excitation of two ENDOR transitions for each of the $M_S = \pm 1/2$ manifolds, as exemplified by the transition labeled b in Figure 3.[12] This is well illustrated in Figure 4 which presents the ENDOR spectra recorded for a crystal orientation of $c||\vec{B}$. In this crystal orientation, the signals of the two types of Mn^{2+} are not resolved. The spectra corresponding to the $M_S = 1/2$ manifold are well resolved, and as expected, selection of the $|-1/2, \pm 5/2\rangle \leftrightarrow |1/2, \pm 3/2\rangle$ transitions produced only one ENDOR peak per manifold, while for the others ^{55}Mn components, two resolved lines appeared.[12] This splitting arises from the second-order contribution of the hyperfine interaction and of the quadrupole interaction, both exhibiting an M_I dependence (see eq 6).
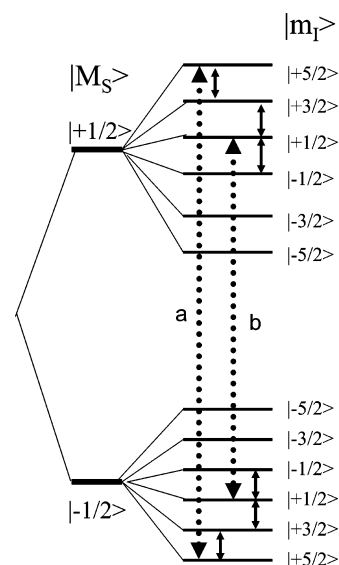
Figure 3. Energy level diagram of Mn^{2+} ion ($S = I = 5/2$) showing only the $M_S = \pm 1/2$ manifolds. The allowed EPR and ENDOR transitions are shown as dotted and solid arrows, respectively. For explanation of the *a* and *b* notations see text.

The explicit contribution of the quadrupole interaction can be obtained from the difference of the appropriate $\Delta \nu$ given in eq 8. Hence, we obtained for this orientation $16F = 4.4$ MHz. Moreover, from $\nu(1/2, 1/2)$ and $\nu(-1/2, 1/2)$, appearing at 169.8 and 92.8 MHz, respectively, $\nu_+ = a_{iso} = -262.5$ MHz is obtained. This value is slightly lower than the one obtained from the EPR spectra, -266 MHz.[5] The different resolution of the ENDOR lines in the $M_S = \pm 1/2$ manifolds is due to the contribution of both the hyperfine and quadrupole terms to the M_I dependence. While the former is M_S dependent, the latter is not (see eq 6), resulting in different splittings and allowing a determination of the sign of F. For $F > 0$ the $M_S = -1/2$ lines should exhibit larger splitting, while for $F < 0$ the $M_S = 1/2$ have larger splittings. For the orientation shown in Figure 4 the $M_S = 1/2$ lines are resolved and therefore $F < 0$.

Example ^{55}Mn ENDOR spectra recorded in the *ac* and *ab* planes and measured at the lowest field hyperfine component ($M_I = -5/2$), tracking the different Mn^{2+} sites when resolution allows, are shown in Figures 5 and 6. These clearly show that the spectra recorded with the magnetic field set to EPR signals of different sites are different. The orientation dependence of the $M_S = \pm 1/2$, and $M_I = -5/2 \rightarrow -3/2$ ENDOR frequencies in the *ac* and *ab* planes are presented in the rotation patterns shown in Figure 7. These show that at some orientations, mainly in the region of the *a* axis (noted by a dashed line in Figure 7) there are more signals than expected for just one type of ^{55}Mn: namely, for each M_S manifold two signals for orientations in the crystallographic planes and one signal when the magnetic field is along the crystallographic axis. The deviations are significantly larger than would be expected from a small misalignment of the crystal. These additional signals are attributed to the presence of two types of Mn^{2+}, which have different nuclear quadrupole tensors as well. To determine the quadrupole tensor and refine a_{iso}, $\Delta \nu$, and ν_+ were calculated and their orientation dependence is presented in Figure 7 as well. The assignment of the ENDOR lines to their respective pairs was derived from the change in their relative intensities upon shifting the field from one resolved feature in the EPR
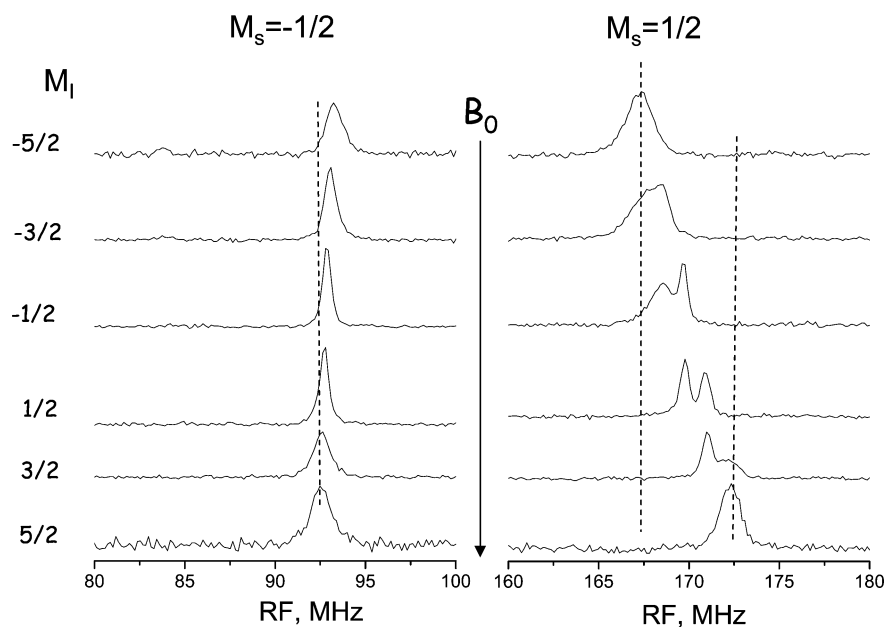
Figure 4. ^{55}Mn ENDOR spectra (6 K) of a concanavalin A single crystal at $c||\vec{B}$ measured at magnetic fields corresponding to all six ^{55}Mn hyperfine components. The dotted vertical lines are drawn to emphasize the relative positions of the signals. The solid arrow marks the increasing direction of the field.
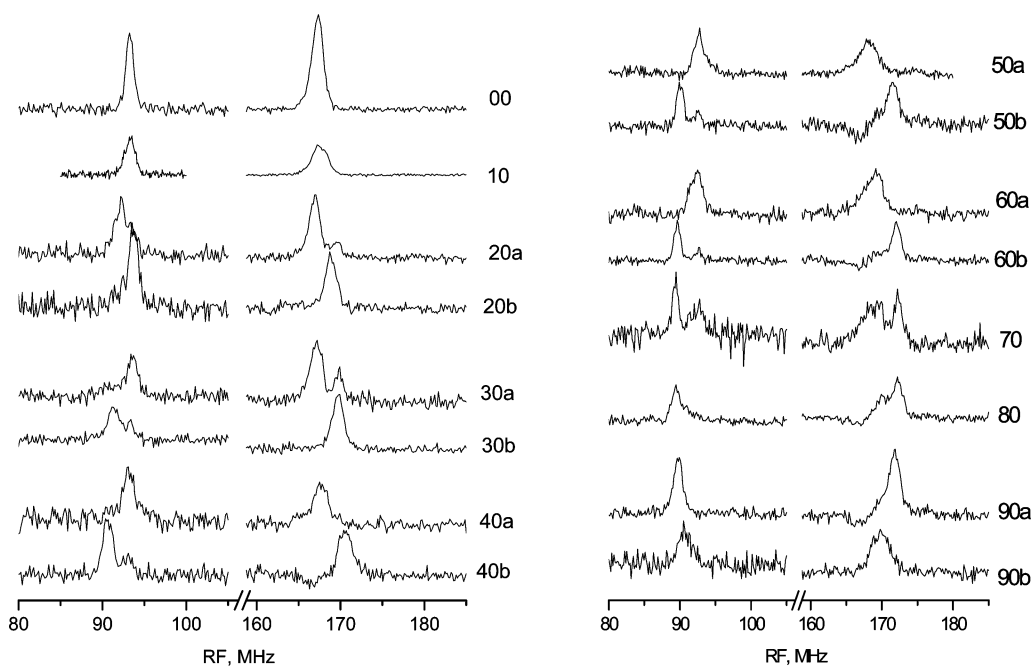

Figure 5. ^{55}Mn Davies ENDOR of concanavalin A for a few selected angular orientations in the *ac* plane, recorded with the field set to the lowest field ^{55}Mn hyperfine component ($M_I = -^5/_2$) and 6 K. The notation *a* and *b* corresponds to resolved EPR features of the different sites.

spectrum to the next, as indicated in Figures 6 and 5 for pairs of spectra noted with *a* and *b*. Moreover, eq 6 shows that the quadrupole interaction causes a related shift (inward or outward) of each individual doublet component with respect to the center of the doublet, thus predicting which lines belong to a particular pair. This argument holds as long as the shift due to the quadrupole interaction is larger than that caused by the hyperfine interaction.

The rotation patterns were simulated by first considering $\Delta\nu$ initially using eq 7 for $M_I = -^5/_2$. Initally, a manual best fit process was carried out to determine the range of the quadrupole tensor parameters, and these were then refined by a best-fit computer program applied to the ENDOR frequencies themselves. This also refined the value of a_{iso}. The distribution of

the points in the ν_+ rotation pattern, confirms that the hyperfine interaction is indeed isotropic, and if anisotropy exists it does not exceed 1 MHz. The rotation patterns of Mn_A^{2+} could be easily tracked, and they were simulated using the parameters listed in Table 2 and shown as solid lines in Figure 7. Considering the rather broad-line width and the S/N of some of the ENDOR spectra, the agreement between the calculated rotation patterns and the experimental points for Mn_A^{2+} is good. The same nuclear Larmor frequency was taken for all orientations. This is justified because the orientation dependence of the individual EPR lines span a maximum of 20 G, which amounts to a variation of 0.02 MHz in ν_I. This is well within the experimental error, in agreement with the ^{1}H ENDOR measurements.
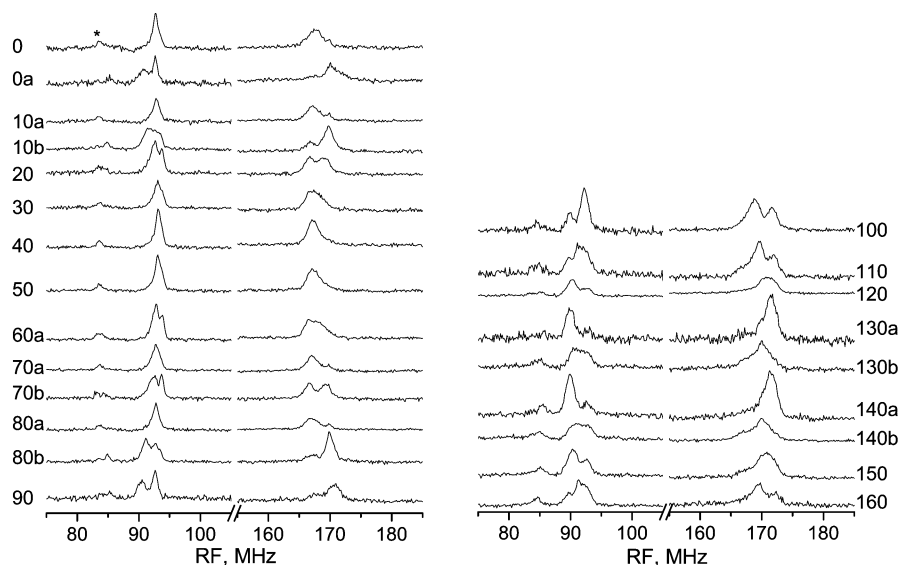
Figure 6. ^{55}Mn Davies ENDOR (6 K) of concanavalin A for a few selected angular orientations in the *ab* plane, recorded with the field set to the lowest field ^{55}Mn hyperfine component ($M_I = -5/2$). The notation *a* and *b* corresponds to resolved EPR features of the different sites. The feature marked with ∗ corresponds to the second harmonic of the $M_S = 1/2$ ENDOR signals and is an instrumental artifact.

The rotation pattern of the $M_S = -1/2$ manifold of the *ab* plane shows also experimental points situated away from the rotation pattern of Mn_A^{2+} that form a line with a very small orientation dependence. These signals, especially those appearing in the $90-160°$ range are clear and resolved. The other rotation patterns reveal similar experimental points, showing little orientation dependence in both *ac* and *ab* planes. These experimental points are attributed to Mn_B^{2+}. Simulations based on these set of points yield a small and negative quadrupole coupling constant and a slightly larger a_{iso} value. The dotted rotation patterns in Figure 7 represent Mn_B^{2+} and its best fit parameters are listed in Table 2. Because of the small anisotropy and the rather broad lines, η and the Euler angles α could not be uniquely determined as for Mn_A, and several options, all with a small negative e^2Qq/h gave a fit similar to that shown in Figure 7. The experimental points in the $M_S = 1/2$ rotation pattern of the *ab* plane noted with a circle, correspond to a weak shoulder and are significantly off the calculated pattern and are therefore probably noise. Taking a larger and positive e^2Qq/h, 0.55 MHz, gives a better fit in the $40-60°$ region of the *ab* rotation pattern, but all the points around the *a* axis in both the *ac* and *ab* plans are too far from the calculated values and therefore we dismissed this option.

Since we know from the analysis of the rotation patterns of the EPR spectra which particular Mn^{2+} site contributes to the ENDOR signals at each observer field, the specific a_{iso}, ZFS, and quadrupolar parameters belonging to the same site were determined. These are all listed in Table 2.

Discussion

The single crystal ^{55}Mn W-band ENDOR measurements showed that at a low temperature there are two inequivalent types of Mn^{2+} in the crystals of concanavalin A, each exhibiting the orientation dependence behavior expected from I_{222} symmetry. The two types exhibit considerably different quadrupole coupling constants, 10.6 versus -2.7 MHz, and slightly different a_{iso} values, -262.5 and -263.5 MHz, respectively. The latter is a small difference but significant because it improves the fit of the ENDOR frequencies of Mn_B significantly. Because of

the symmetry properties of the crystal there are four possibilities to orient the quadrupole tensor with respect to the 3D crystal structure. None of the four possibilities for Mn_A^{2+} shows a clear orientation of one of the principal axes along a Mn–ligand direction. This is somewhat surprising because the deviation from local octahedral symmetry, in terms of bond lengths and orientations, is small, although the asymmetry can be attributed to different charges. Four of the Mn–O distances, forming an equatorial plane (see Figure 2) are rather close (2.15 Å for asp10, 2.18 Å for W_{413}, 2.17 Å for glu8, and 2.19 Å for asp19) while the Mn–N and Mn–O_{412} are longer (2.23 and 2.26 Å, respectively). In addition, ligand–Mn–ligand angles show a maximum deviation of 5 from 90°, except for O_{413}–Mn–asp19 which is 81.1°.[9] Asp19 is a bridging ligand with the Ca^{2+} site, which may be the reason for the larger distortion. From all four possibilities, the *z* principal axis of Mn_A^{2+} in site 4 (see Table 1) was found to be 25° of the Mn–asp10 direction, as shown in Figure 8. In contrast to that of Mn_A^{2+}, the small quadrupole coupling constant of Mn_B^{2+} resulted in a small anisotropy, which could not be well resolved because of the experimental error, and therefore the orientation of the tensor could not be determined very precisely. Nonetheless, for all four possibilities the principal *z*-axis was not found close to any of the Mn–ligand directions. Interestingly, for site 4 the *z*-axis of Mn_B^{2+} makes an angle of 30° with Mn–asp19, exhibiting a 90° rotation as compared to Mn_A (see Figure 8). Asp10 and asp19 are the amino acids that also binds the Ca^{2+}, which is close to the sugar-binding site. This rotation of the *z*-axis is in line with our earlier suggestions that the conformational equilibria involves a carboxylate from asp10 or asp19.[5] Unfortunately, it is not possible to carry out pulse ENDOR measurements at room temperatures, and therefore the average quadrupole tensor could not be determined to further confirm the presence of the conformational equilibrium. Moreover, we did not find any carboxylate with a larger thermal atomic displacement ellipsoid in the X-ray diffraction data that could be correlated with the change in the size of the principal components of the quadrupole tensor.[9]
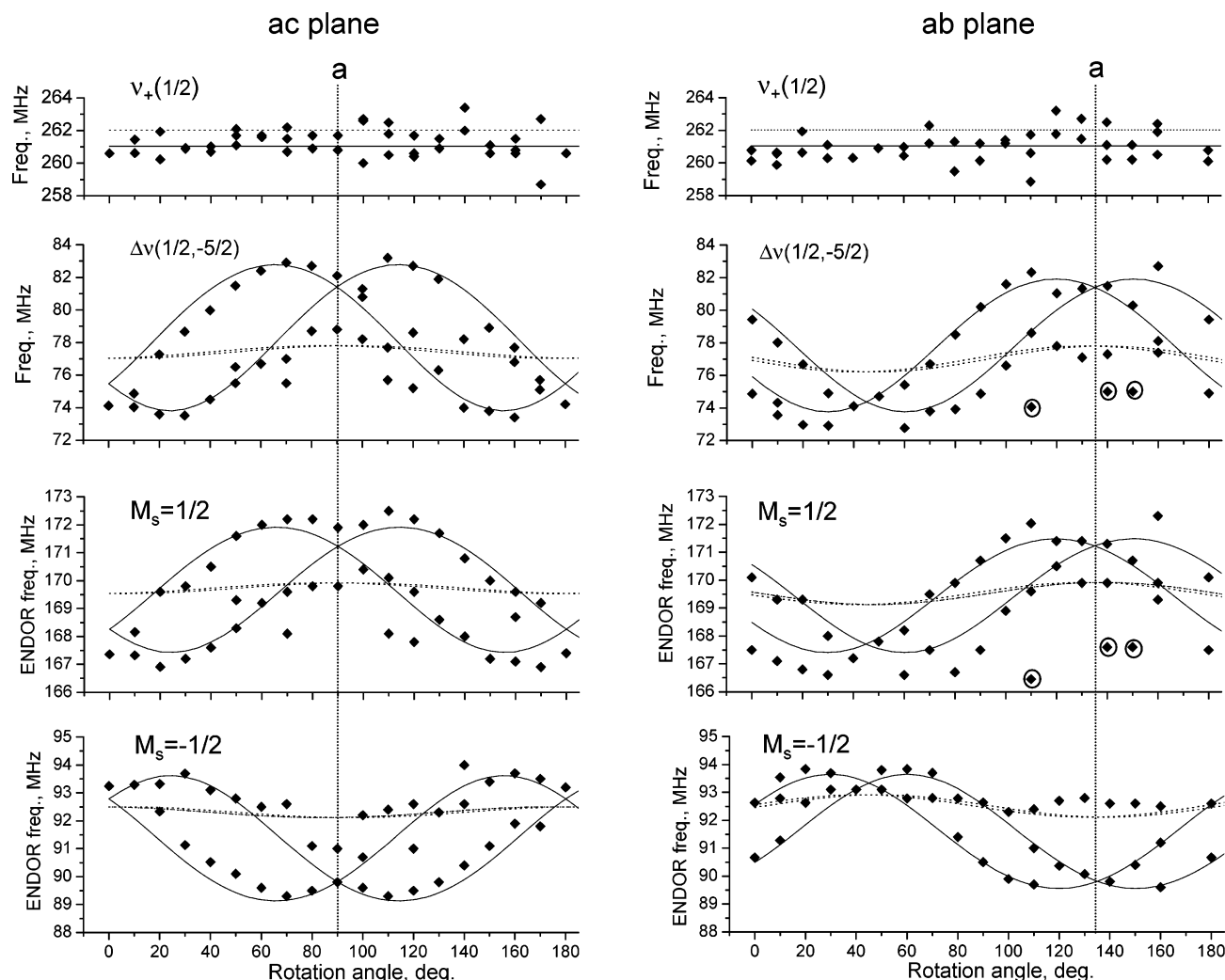
Figure 7. Rotation patterns of the ENDOR frequencies of the $M_I = -5/2$ component within $M_S = \pm 1/2$ manifolds and of the corresponding $\nu_+ (1/2, -5/2)$ and $\Delta\nu(1/2, -5/2)$ in the *ac* and *ab* planes. The dotted vertical lines mark the positions of the crystallographic *a* axis. The solid ($^{55}Mn_A^{2+}$) and dashed ($^{55}Mn_B^{2+}$) lines were simulated using the parameters listed in Table 2; $B_0 = 3.36$ T was used in the simulations. For the circled data points, see text.

Table 2. The Best Fit Hyperfine and Quadrupole Parameters of the ^{55}Mn ENDOR Spectra as Obtained from the Simulations along with the *D* and *E/D* Values Obtained from the EPR Analysis[5] [a]

Mn sites	e^2Qq/h MHz	η	α	β	γ	a_{iso}, MHz	*D*, MHz[5]	*E/D*[5]
Mn_A^{2+}	10.7 ± 0.6	0.15 ± 0.05	130 ± 5	105 ± 5	155 ± 10	-262.5 ± 0.2	789	0.24
Mn_B^{2+}	-2.7 ± 0.6	0.0 ± 0.3	[b]	35 ± 10	85 ± 10	-263.5 ± 0.2	970	0.145

[a] The angles are with respect to the (*c, a, b*) crystal system (in deg). [b] For $\eta = 0$, α can be any angle.

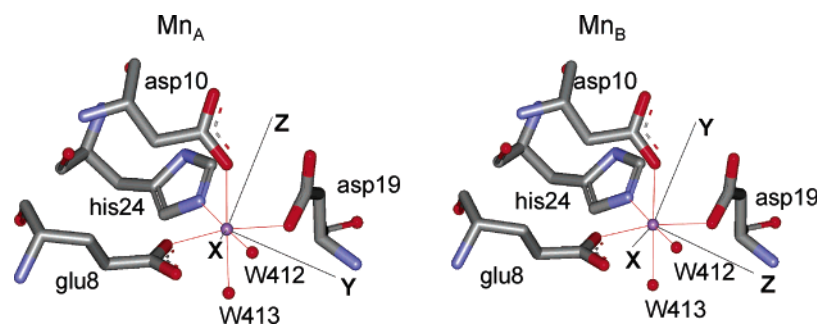**Figure 8.** One of the four possibilities of the orientations of the quadrupole tensor of $^{55}Mn_A^{2+}$ and $^{55}Mn_B^{2+}$ with respect to the crystal structure.[9]

Information about the quadrupole coupling constant of $^{55}Mn^{2+}$ and the tensor orientation with respect to the atomic coordinates of the ligands is rather scarce, and most of the reports concern highly symmetric inorganic crystals, into which

Mn^{2+} has been doped. In these cases, the atomic coordinates are obtained from the pure crystal because the distortions introduced by the doping cannot be determined by X-ray diffraction. The e^2Qq/h values of ^{55}Mn for the two sites of Mn^{2+}

in La$_2$Mg$_3$ (NO$_3$)$_{12}$·24H$_2$O are 2.56 and 1.49 MHz.[27] The value obtained for Mn^{2+} doped in FeBr$_2$ is a little higher and amounts to 3 MHz.[28] These values are close to that of Mn$_B^{2+}$ but considerably smaller than that of Mn$_A^{2+}$. Considerably higher values, 35.5 and 41.4 MHz, were obtained for two Mn$_{12}$ single-molecule magnets.[29] ⁵⁵Mn ENDOR measurements carried out at X-band on isolated Mn^{2+} ions in a bulk ZnGeP$_2$ crystal gave $e^2Qq/h = 12.4$ MHz.[30] No information was given regarding the orientation of the tensor. The effect of the quadrupole interaction on the X-band CW ENDOR spectrum was also noted for CdS/Mn(II) nanocrystals from which a quadrupole constant of 1 MHz was derived.[31] Randall et al.[32] reported for a Mn(III)Mn(IV) complex rather large quadrupole couplings, −26.7 and −60 MHz, respectively. Since the latter was determined from a frozen solution there is no information regarding the orientation of the tensor.

It is interesting to compare the ZFS and the quadrupole tensors, although their origins are different. The nuclear quadrupole interaction is primarily determined by the charge distribution in the Mn^{2+} site, namely the position and character of the ligand atoms. The ZFS, in turn, is determined by the orbitals occupied by the unpaired electrons and includes also contributions of excited states via the spin−orbit coupling.[33] We have found no close correlation between the tensors orientations, although in both cases they are not along any of the Mn−ligand axes. Moreover, while Mn$_A$ has the larger e^2Qq/h value, it exhibits the lower D value (see Table 2). There is also no correlation between the asymmetry parameters of the two tensors, while the quadrupole tensor η was found to be rather small for the two sites, for the ZFS splitting it is substantial, considering that $3E/D = \eta$. The lack of correlation between the ZFS and ⁵⁵Mn quadrupolar parameters was noted for Mn^{2+} in La$_2$Mg$_3$(NO$_3$)$_{12}$·24H$_2$O as well.[27]

The structure of concanavalin A with the bound saccharide shows a close contact of the saccharide, through a hydrogen bond, with the nitrogen of asn14, where the adjacent carbonyl is the Ca^{2+} ligand opposite the asp10 ligand.[34] Hence, one can envision a relay between the saccharide binding and a possible displacement of the carboxylate of asp10. It was therefore suggested that the motion observed manifests some residual freedom, which exists to facilitate the binding of the saccharide.[5] This, then suggests that upon the saccharide binding only one site will predominate at low temperatures. To verify this hypothesis we grew cubic crystals of concanavalin A bound with α-D-methyl glucopyranoside, but unfortunately our attempts to flash freeze the crystals using a variety of cryo-protectants that do not dissolve the crystals and retain its integrity upon freezing failed.

Calculations of the efg Tensor. To account for the structural origin of the different e^2qQ/h values of Mn$_A$ and Mn$_B$ (factor of 4) we applied a simple point charge model (PCM) used to calculate the efg tensors of metal ions in ionic solids.[35,36] The atom positions were taken from the crystal structure of the protein, which we considered as some average of the two sites. Because of the simplicity of the model we do not attempt to apply it for the determination of the geometry of the two different sites by fitting the magnitude and orientation of the tensors, but rather to explore the sensitivity of the efg principal value to minor charge variations and small displacements of a particular ligand. This, in turn, provides insight to the amplitude of the variations required to induce the relative differences observed experimentally in e^2qQ/h.

According to the PCM, the quadrupole tensor is given by[35]

$$\mathbf{P} = \frac{eQ}{h2I(2I-1)}(1 - \gamma_\infty)e\mathbf{q} \qquad (11)$$

where eq represents the contributions to the efg from the lattice and γ_∞ is the Sternheimer antishielding factor.[38] It accounts for distortions induced in the core electrons by the external-field gradients. The elements of e**q** are given by

$$eq_{\alpha\beta} = \frac{e}{4\pi\epsilon_0}\sum_{i=1}^{n}Z_i\frac{3\alpha\beta - r^2\delta_{\alpha\beta}}{r^5} \qquad (12)$$

where the index i refers to the i'th atom around the Mn^{2+}, Z_i is its charge, and α, $\beta = x, y, z$ are its coordinates. The contribution from valence electrons, eq$_{val}$, has been neglected in eq 12. While this may be valid for ions with closed shell such as Ca^{2+},[40] it may not be for Mn^{2+} with a half-filled shell. The principal components are the eigenvalues of e**q**, and the eigenvectors provide the relative orientation with respect to the crystallographic frame of reference. Multiplication of the principal values by $(eQ/h2I(2I-1))(1 - \gamma_\infty)$ yields P_{xx}, P_{yy}, and P_{zz}. When the efg is given in atomic units and the nuclear quadrupole moment is in barn (= 10^{-28} m^2), a conversion factor of 234.96 yields e^2qQ/h in MHz.[39] The calculated Sternheimer factor of Mn^{2+} is −11.4,[38] and this value was employed in the calculation of the quadrupole coupling constant of Mn^{2+} in MgO.[41] There the point-charge model was applied, neglecting eq$_{val}$, and a good agreement between calculation and experiment was obtained.

Equation 12 shows that the efg is affected both by the positions and charges of the Mn^{2+} neighboring atoms. Two of the carboxylate ligands, asp10 and asp19, are bridging ligands (see Figure 1). One oxygen is coordinated to the Mn^{2+} and the other to the Ca^{2+}, hence a possible competition between the two metal cations on the negative charges can be envisioned,

(27) De Beer, R.; Van Ormondt, D. *Phys. Lett. A* **1968**, *27*, 475−476.
(28) King, A. R.; Merle-d'Aubigné, Y.; Rezende, S. M.; Soares, E. A. *Phys. Rev. B* **1978**, *18*, 4598−4605.
(29) Harter, A. G.; Chakov, N. E.; Roberts, B.; Achey, R.; Reyes, A.; Kuhns, P.; Christou, G.; Dalal, N. S. *Inorg. Chem.* **2005**, *44*, 2122−2124.
(30) Garces, N. Y.; Halliburton, L. E.; Schunemann, P. G.; Setzler, S. D. *Phys. Rev. B* **2005**, *72*, 033202−4.
(31) Hofmann, D. M.; Hofstaetter, A.; Leib, U.; Meyer, B. K.; Counio, G. *J. Cryst. Growth* **1998**, *184/185*, 383−387.
(32) Randall, D. W.; Sturgeon, B. E.; Ball, J. A.; Lorigan, G. A.; Chan, M. K.; Klein, M. P.; Armstrong, W. H.; Britt, R. D. *J. Am. Chem. Soc.* **1995**, *117*, 11780−11789.
(33) Neese, F. *J. Am. Chem. Soc.* **2006**, *120*, 10213−1022.
(34) Bradbrook, G. M.; Gleichmann, T.; Harrop, S. J.; Habash, J.; Raftery, J.; Kalb (Gilboa), J.; Yariv, J.; Hillier, I. H.; Helliwell, J. R. *Faraday Trans.* **1998**, *94*, 1603−1611.

(35) Marichal, C.; Kempf, J. Y.; Maigret, B.; Hirschinger, J. *Solid State NMR* **1999**, *8*, 33−46.
(36) Han, O. H.; Oldfield, E. *Inorg. Chem.* **1990**, *29*, 3666−3669.
(37) Lucken E. A. C. *Nuclear Quadrupole Coupling Constants*; Academic Press: London, New York, 1969.
(38) Sternheimer, R. M. *Phys. Rev.* **1963**, *130*, 1423−1425.
(39) Sinnecker, S.; Neese, F.; Noodleman, L.; Lubitz, W. *J. Am. Chem. Soc.* **2004**, *126*, 2613−2622.
(40) Troniker, A.; Bellot, P.-V.; Zhdanov, Y.; Yakubovskii A. *Solid State NMR* **2000**, *16*, 171−175.
(41) Stroubeck, Z.; Simanek, E.; Orbach, R. *Phys. Rev. Lett.* **1968**, *20*, 391−392.
(42) Blakeley, M. P.; Kalb, A. J.; Helliweill, J. R.; Myles, D. A. A. *Proc. Natl. Acad. Sci. U.S.A.* **2004**, *101*, 16405−16410.

Table 3. The Z_i Values Used in the efg Calculations

atom	charge	atom	charge	atom	charge
Mn	1.627				
glu8($O_{\epsilon2}$)	−0.84	glu8($O_{\epsilon2}$)	−0.61	glu8(C_ϵ)	0.77
asp10($O_{\delta2}$)	−0.78	asp10 ($O_{\delta2}$)	−0.87	asp10($C_{\delta2}$)	0.79
asp19 ($O_{\delta1}$)	−0.86	asp19 ($O_{\delta1}$)	−0.85	asp19(C_δ)	0.80
his24($N_{\epsilon2}$)	−0.61	his24($C_{\delta1}$)	−0.096	his24($C_{\epsilon2}$)	0.13
O_{w412}	−1	H_{w412}	0.525	H_ϵ	0.22
O_{w413}	−1	H_{w412}	0.525	H_δ	0.26

leading to two conformations, relatively close in energy, differing in their Mn−O distances, orientations, and the charges on the oxygen ligands. This hypothesis is further supported by the direction of the z-axis of the Mn_A tensor which is pointing close to the Mn−O(asp10) direction, and a reduction e^2qQ/h should involve asp10. Recent 15 K neutron diffraction measurements on concanavalin A reported high disorder for one of the water ligands.[42] [1]H ENDOR measurements, however, showed that Mn_A^{2+} and Mn_B^{2+} have the same spectra, thus excluding the involvement of the water and histidine ligands in the dynamics. Accordingly, in the calculations we limited the changes to asp10 and asp19.

The charge distribution in a protein metal site is not as obvious as in an ionic crystal, and therefore the charges on the various atoms are the formal usual charges. Therefore they were obtained from a single point DFT calculation using the crystal-structure coordinates. The calculations were carried out on a cluster of 89 atoms, including protons, considering all ligands of Mn^{2+} and Ca^{2+}, truncated at the β carbon (for asn14 the γ carbon), which was terminated with a methyl group, and protons were added. The multiplicity was 6 and the total charge of the cluster was 2+ (Ca= 2+, Mn= 2+, one negative charge on each of the three carboxylates of glu8, asp19, and asp10, and one positive charge on asn14).

In the efg calculations a total of 20 atoms (eq 12) around the Mn^{2+} were taken into account, including the two oxygens and the carbon of the three carboxylates, the coordinated nitrogen, the two closest histidine carbons, their protons, and the water atoms, the charges of which are listed in Table 3. The charges are similar to those obtained by Spiegel et al.[42] for Mn catalase and the denovo protein DF1, which features a binuclear Mn(II) with charges close to −0.7 on the carboxylates and the glutamate and +1.62 on the Mn. With the use of the charges in Table 3 and the coordinates of the atoms, the efg was computed, exploring particularly the dependence of eq_{zz} on the charge and position of the Mn^{2+} coordinated oxygen atoms of asp10 and asp19.

The effect of the Mn−O(asp10) distance variation in the range $r_0 \pm \Delta r$, $\Delta r \pm 0.2$, holding all other parameters constant, on eq_{zz} and η is presented in Figure 9a. It shows a change of about 50% in eq_{zz} and a similar change is produced by the charge variation (Figure 9b). Here the total charge of the two asp10 oxygen atoms was kept constant. Variations of the Mn−O orientation over a cone (with constant r_0) of $\theta = 20°$ about the original Mn−O direction, as a function of the azimuthal angle ϕ within the cone can increase eq_{zz} by about 70% (Figure 9c). All these changes show that variation of a single parameter can lead to a maximum change of 70% which is well below the experimental observation. Figure 9 also shows that the asym-

(43) Spiegel, K.; De Grado, W. F.; Klein, M. L. *Proteins: Struct., Funct., Bioinfo.* **2006**, *65*, 317−330.

metry parameter, η, is most sensitive to variations in the orientation. We also verified the effect on the angle between the z-axis and the Mn−O(asp10) direction, which for the crystal structure is 10°. Here an abrupt change to about 90° was observed, while changes in the orientation of the bond span a wide range of angles (not shown). The same calculations were carried out for asp19 and the results are also shown in Figure 9. Here the effects on eq_{zz} are significantly milder, but η changes considerably. When η is close to 1, the choice of the z and x is actually arbitrary, and this is the reason for the abrupt change of the sign of eq_{zz}.

The experimental results show a difference of a factor of 4 and a sign change for eq_{zz}. This large change requires the variation of more than a single parameter. Accordingly, we searched for the maximum and minimum eq_{zz}, $eq_{zz}(max)$, and $|eq_{zz}(min)|$, within the range of $r_0 \pm 0.2$ Å, $\theta = 0-30°$ ($\phi = 0-360°$) and a Z_O range of −0.5 to −1. The results are summarized in Table 4. Limiting Δr to ±0.1 did not generate a small negative eq_{zz}. The values in Table 4 show that for asp10 the difference between $eq_{zz}(max)$ and $|eq_{zz}(min)|$ span a larger relative range than obtained experimentally. In addition, we found that there is a relatively broad range of small variations from the crystal structure for which $eq_{zz} = 4|eq_{zz}(min)|$ and $\eta = 0.15 \pm 0.05$ that can be attributed to Mn_A. In contrast, a negative small $eq_{zz}(min)$ for Mn_B, could be obtained by a very narrow range of parameters, with a significantly larger deviation from the crystal structure. Moreover, for these the calculated η is significantly overestimated, even after considering the large experimental error. A similar behavior is obtained for asp19, but the range of geometrical changes that reproduce the relative magnitudes of the eq_{zz} values is significantly narrower than for asp10. Therefore, involvement of asp10 in the conformational dynamic is more likely. Interestingly, the structural variations in the range tested also result in a reorientation of the z-axis as observed for Mn_A and Mn_B.

The eq_{zz} and η values obtained for the crystal coordinates without any distortion are listed in Table 4 as well. Using the Sternheimer factor and a Q value of 0.4 barn for Mn^{2+}, e^2qQ/h was calculated (see Table 4) and compared to the value obtained from the single point DFT calculations. The PCM value is overestimated by a factor of about 2. In addition, there is a large difference in the value of η, from almost axial symmetry for PCM to very high rhombicity for the DFT. The high rhombicity also introduces an ambiguity in the sign because small changes lead to an exchange of x and z. The magnitude of the DFT e^2qQ/h is closer to the experimental value for Mn_A, while η is highly overestimated. The overestimation η of e^2qQ/h produced by the PCM is pronounced also for the maximum and minimum e^2qQ/h (see Table 4) with respect to the experimental values. One possibility for the discrepancy can be an overestimated γ_∞. For example, a recent report of the experimental determination of γ_∞ of Ca^{2+} showed that the calculated value was overestimated by a factor of 3.[41]

[55]Mn quadruple coupling of Mn(IV)/Mn(III) model compounds were calculated by DFT. The sign of P_{zz} was well reproduced for both Mn(III) and Mn(IV), and its magnitude was on the order of the experimental values, with deviations reaching up to 100%. The values obtained, however, were significantly larger than in our case.[39] It is interesting to compare the eq values obtained from the point-charge calculation with that
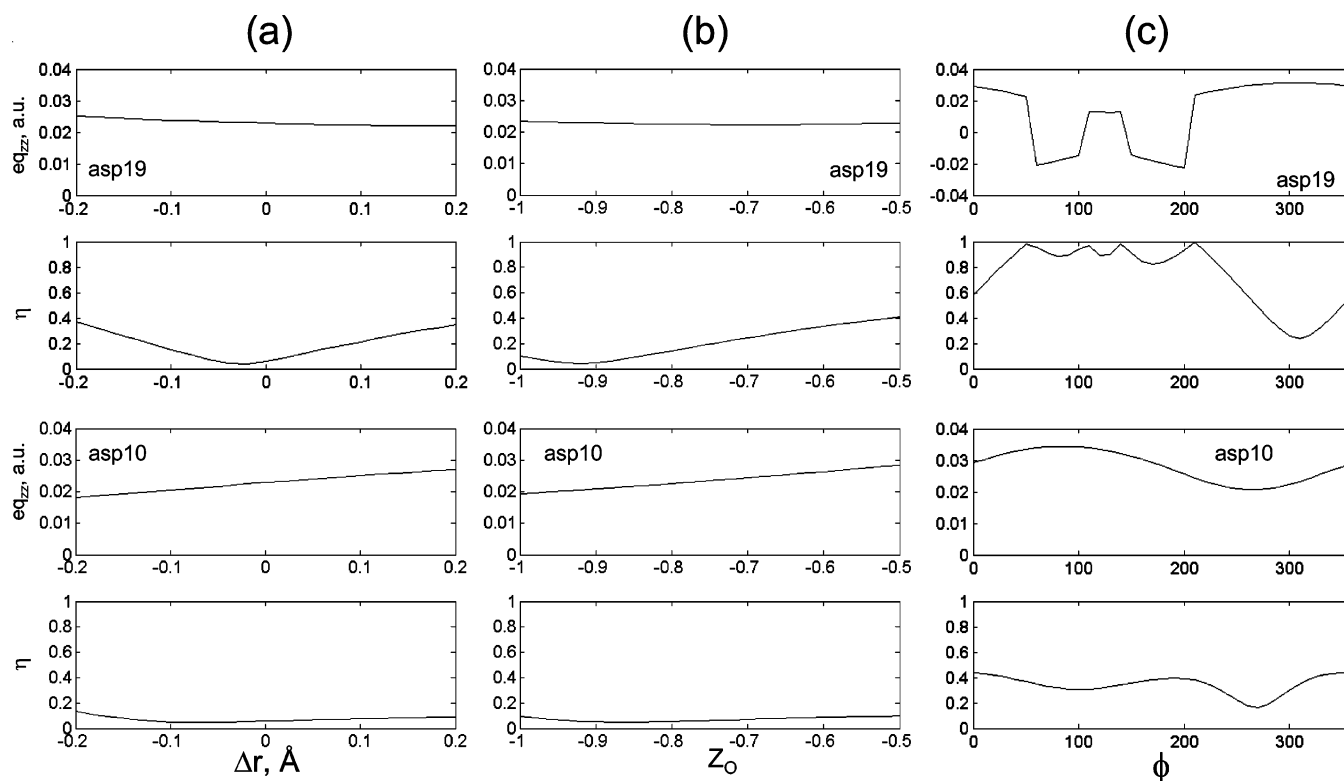
Figure 9. The dependence of the calculated ^{55}Mn^{2+} eq$_{zz}$ and η for variations in (a) distance, (b) charge, and (c) orientation of the coordinated oxygen atoms for $\theta = 20°$ of asp10 and asp19.

Table 4. The Parameters of the Mn−O Bond of asp10 and asp19 That Yield a Maximum and Minimum $|e^2qQ/h|$ and the Associated η Value

	crystal structure[a]	asp10 eq$_{zz}$(max)	asp10 eq$_{zz}$(min)	asp19 eq$_{zz}$(max)	asp19 eq$_{zz}$(min)
Z_o		−1.0	−1.0	−1.0	−0.72
Δr, Å	0	−0.2	−0.2	−0.2	−0.2
θ	0	30°	15°	30°	30°
ϕ	0	110°	260° (250°)[b]	230°	130°
eq$_{zz}$, au	0.023 (−0.153)[c]	0.0435	0.005 (−0.006)	0.04	−0.01
η	0.06 (0.89)[c]	0.82	0.78 (0.94)	0.7	0.95
e^2qQ/h, MHz	26.8 (−14.4)[c]	50.7	5.8 (−7.0)	46.6	−11.7

[a] The charges are given in Table 3. [b] The values in parenthesis represents parameters that yield a the minimum $|e^2qQ/h|$ for negative values. [c] The values obtained from single-point DFT calculations using B3LYP.

calculated from the DFT for the same structure on the basis of the crystal structure. Neglecting the contributions from the charge distribution of the Mn^{2+} itself and of electron density shared between the metal and the ligand, the DFT calculation produced eq$_{zz}$ = 0.055 au and η = 0.39 to be compared with eq$_{zz}$ = 0.023 au and η = 0.06 from the PCM. Here the point charge approximation underestimates eq$_{zz}$.

In addition to the approximation of using a simple ionic model, our calculations have additional limitations: the movement of the single atom was decoupled from the other atoms on the residue, which, although the displacement was small, could lead to nonrealistic bond angles and distances for its neighbors. For example, small movement of one of the carboxylate oxygens should change the position of the second oxygen; however, because this oxygen is more distant from the Mn^{2+}, this effect on the efg should be small. More important is the correlation between the position of a coordinated oxygen and the charge distribution, which we did not account for. These can be obtained by more sophisticated types of calculations,

such as DFT. Nonetheless, the SPM calculations support the hypothesis that the difference between Mn$_A$ and Mn$_B$ originates from two conformations of the bridging ligands, more specifically, asp10. They also show the limitation when applied to metal ions in proteins and show the necessity for elaborate and systematic DFT calculations providing the dependence of the quadrupole coupling constant, asymmetry parameter, and orientation on small geometric changes in these ligands, along with the energetics involved, which are known experimentally.[5]

Conclusions

It was shown for concanavalin A that the Mn^{2+} ZFS does not introduce anisotropy into the W-band ENDOR frequencies, and the observed orientation dependence of the ^{55}Mn ENDOR signals is due to the nuclear quadrupole interaction. The two types of Mn^{2+} sites, Mn$_A^{2+}$ and Mn$_B^{2+}$, resolved earlier in the EPR spectra, were found to have significantly different quadrupole coupling constants, 10.6 and −2.7 MHz, respectively. In addition, a small difference, of 1 MHz, was also detected in their hyperfine couplings. The principal z-axis of Mn$_A^{2+}$ is not aligned with any of the Mn−ligand directions, but was tilted 25° degrees away from Mn−O(asp10), and its orientation is different than that of the corresponding ZFS z-axis. A similar observation was found for Mn$_B^{2+}$, with the z-axis pointing 30° away from the Mn−O(asp19) direction, rotated about 90° from that of Mn$_A^{2+}$. These results show, that similar to the ZFS, the quadrupolar interaction is highly sensitive to small differences in the coordination spheres of the Mn^{2+}. This was not detected by the high-resolution X-ray crystallography and is in agreement with the earlier observation of a conformational dynamic detected through the ZFS interactions, which is frozen out at low temperatures and averaged at room temperature.

Calculations of the quadrupole tensor using the point-charge model suggest that a relatively small displacement of the oxygen ligand of asp10 can lead to differences of the order observed experimentally.

Supporting Information Available: Expressions of the ENDOR frequencies for $S = {}^5/_2$, $I = {}^5/_2$ up to third order in the ZFS, not including the quadrupole interaction and calculation of the orientation dependence of the ENDOR frequencies for Mn(II) at W-band with the ZFS of concanavalin A. This material is available free of charge via the Internet at http://pubs.acs.org.

JA0662826